Polarized Raman study of the phonon dynamics in $Pb(Mg_{1/3}Nb_{2/3})O_3$ crystal

Oleksiy Svitelskiy* and Jean Toulouse
Department of Physics, Lehigh University, Bethlehem, PA 18015, USA

Z.-G.Ye
Department of Chemistry, Simon Fraser University, Burnaby, BC, V5A 1S6, Canada

$Pb(Mg_{1/3}Nb_{2/3})O_3$ is one of the simplest representatives of the class of lead relaxors and often serves as a model system for more complicated compounds. In this paper we analyse both polarized and depolarized Raman scattering spectra, measured in the temperature range between 1000 and 100 K, by multiple peak decomposition. Basing on this analysis, we present the picture of transformations in the crystal and the nature of the spectral lines. According to our model, the formation of the Fm3m symmetry in the chemically ordered regions as well as the appearance and freezing of the polar nanoregions are the consequences of the same phenomenon: ion off-centered displacements and their reorientational thermal motion. The lowering temperature progressively limits this motion from eight to four, two and only one site. Raman scattering exists due to the presence of the Fm3m and polar clusters. It is a product of the multiphonon interaction process, mediated by the presence of the dynamic and static disorder.

I. INTRODUCTION

$Pb(Mg_{1/3}Nb_{2/3})O_3$ (PMN) is one of the earliest members of the growing family of lead ferroelectric relaxors, which, due to its application potential, has been attracting attention of researchers for many years. However, despite significant efforts, many properties of lead compounds are still unclear and the very nature of the relaxor behavior has yet to be understood. The difficulties stem from the high complexity of these materials with a high degree of compositional, chemical and structural disorder.

$Pb(Mg_{1/3}Nb_{2/3})O_3$ has a perovskite structure with, on average, a cubic Pm3m symmetry, with Mg^{2+} and Nb^{5+} ions interchanging on B sites. Measurements of the dielectric constant show that the crystal does not undergo a sharp transition to a ferroelectric phase. Instead, the dielectric constant exhibits a broad maximum at $T_{max} \sim 270$ K[1]. Below $T_d \sim 620$ K, it deviates from Curie-Weiss law[3] and, at $T \lesssim 350$ K, exhibits strong dispersion[2]. The structure of PMN is not homogeneous. If Mg and Nb occupation ratio were uniformly and ideally equal 1:2 throughout the crystal, it would have a rhombohedral symmetry R3m. But, a network of superstructure clusters with face centered cubic symmetry (Fm3m), destroys the picture. The size of these clusters is of the order of 2-3 nm; the distance between the centers of the neighboring clusters is near 2.5 nm[4,5].

The most widely accepted hypothesis, so-called "space-charge model", associates these Fm3m clusters with antiferroelectrically ordered[6] areas where Mg:Nb occupation ratio is equal to 1:1, i.e. with local composition $Pb(Mg_{1/2}Nb_{1/2})O_3$[7,8]. Such 1:1 clusters carry an excessive negative charge, which is compensated by the positively charged host matrix. Network of these charges acts as a source of random fields and may prevent the occurrence of the "normal" phase transition. Alternatively, the Fm3m clusters might be explained by the local order in the form of $Pb[B^{2+}_{1/2}B^{5+}_{1/3}]_{1/2}[B^{5+}]_{1/2}O_3$[9,10]. This hypothesis avoids assumption of the considerable space charges and calls for other reasons to explain relaxor behavior, including the random fields due to the disorder-induced local anisotropy[11], effects related to different ionic radii[12] or both[13].

The presence of areas with special order causes crystalline structure to change in an intricate way. At the high temperature limit, the crystal has a uniform primitive cubic (Pm3m) structure. Lowering the temperature leads to distinguishability between Mg^{2+} and Nb^{5+} sites and to formation in the ordered regions of a face centered (Fm3m) superstructure. The temperature of the Fm3m clusters formation has yet to be determined. Husson's data suggests they presence at T∼850 K[14]. Our data (see below) raise the upper limit to a temperature higher than 1000 K.

Cooling the sample leads to the nucleation of polar nanoregions (PNR's) characterized by the local distortions. These distortions are responsible for the deviation of the dielectric constant from Curie-Weiss law at T_d[3]. Their presence also causes a non-linearity in the temperature dependence of the optical refraction index[15]. Size of the PNR's is equal to 30-80 Å depending on temperature[16]. The appearance of polar distortions is a consequence of the ion off-centering that is a common property of many perovskites. By structural similarity, one could expect that the mechanism of the polar regions formation in PMN is analogous to the one in $KTa_{1-x}Nb_xO_3$ (KTN)[17]. However, unlike KTN where Nb^{5+} is the only off-centered positive ion, PMN represents a more difficult case. Here, not only *both ions of B-type*, Mg^{2+} and Nb^{5+}, are shifted by ∼0.1-0.2 Å, but also Pb^{2+}, *ion of A-type*, is off-centered by ∼0.25-0.35 Å[18,19,20,21,22]. The B-ions tend to shift along a (111) direction, thus having eight equivalent positions. The shifts of the Pb^{2+}-ions exhibit a spherically symmetric distribution[22]. It is often assumed[11,12,13,14] that Nb^{5+},

TABLE I: Interpretations of Raman scattering spectrum from PMN offered by various research groups. Note, many of the entries in the table mutually exclude each other.

Research Group	45 cm^{-1}	130 cm^{-1}	260 cm^{-1}	420 cm^{-1}	500-600 cm^{-1}	780 cm^{-1}
Husson[14] (1990)	Pb-O stretching modes		O-B-O bending	Mg-O-Mg stretching	Nb-O...Nb stretching	Nb-O...Mg stretching
Dimza[41] (1992)						Coexistence of tetragonal and rhombohedral phases
Krainik[26] (1993)	TO_1					
Idink[40] (1994)	All spectrum is due to one phonon processes, originates from rhombohedral symmetry clusters and consists of 9 modes					
Marssi[27,28,29,30] (1996-98)	TO_1	TO_2	TO_3	TO_4		TO_2+TO_4 or LO_4 (1996) Nb-O-Mg or LO_4 (1998)
Jiang[32] (1999)	Due to positional disorder of lead			Due to Fm3m clusters and vibration of oxygen octahedra		
Lushnikov[33,34] Siny[35,36,37,38,39] (1999)	All spectrum originates from Fm3m clusters, similarly to the case of $PbSc_{1/2}Ta_{1/2}O_3$ VV-E_g?? VH-2T_2g or VV and one VH have fractal character another VH-T_{2g}		Disorder-induced scattering from silent modes and second-order scattering			A_{1g} Breathing mode of oxigen
Dujovne[31] (2002)	TA+disorder					

due to its position in the cell and small radius, acts as the main ferroelectric agent.

At high temperature, the off-centered ions are free to reorient among all allowed off-centered positions. Cooling down and the growing role of the electric interactions causes the appearance of correlated regions consisting of several neighboring cells. Each such region is characterized by a giant electric dipole moment and a local distortion from the cubic symmetry. The PNR's are capable of reorientational motion as whole units. In KTN, the development of these regions leads, at some critical temperature, to a phase transition. However, in PMN, the polar regions develop under constraints imposed by the local anisotropy. As a result, no ferroelectric phase transition, but a glasslike freezing of the polar regions is observed[11]. A bias electric field of magnitude ~ 1.8 kV/cm, applied in the (111) direction, is sufficient to compensate for the influence of the frustrating effects and to induce, at $T_{do} \sim 210$ K, a transition to the rhombohedral R3m ferroelectric phase[23].

Raman spectra of PMN have been measured and reported by several research groups[14,24]. But, the high complexity of the processes caused difficulties in their interpretation, especially due to possible coexistence of clusters with Pm3m, Fm3m and R3m symmetry. It has been shown that the major spectral lines are of first-order character[25]. In cubic crystals first-order Raman scattering is prohibited by symmetry. Explanation of the appearance of first-order scattering *in principle* is the one side of the problem. Another side is the assignment of *particular* lines. The question of the soft ferroelectric mode (TO_1) and the strong Raman line at $\sim$45 cm^{-1}, which is close to where the TO_1 is expected to be found, has been like a stumbling block for investigators. Interpretations of the PMN Raman spectrum offered by various research groups are summarized in Table I. This table reflects the variety of mutually excluding opinions ranging from those that explain the light scattering by *disorder in general* (groups of Husson[14], Krainik[26], Marssi[27,28,29,30], Dujovne[31]) to those that connect it to the presence of some *particular type of disorder*, the one that can lead to the appearance of clusters with symmetry allowing first-order scattering, like face centered cubic (Jiang[32], Lushnikov[33,34], Siny[35,36,37,38,39]), rhombohedral (Idink[40]) or tetragonal (Dimza[41]). The assignement of particular lines is even more contradictory. Recently made first-principle calculations[42] can confirm only few of them. We believe, the arguments might be resolved by taking into account the possibility of coexistence of different mechanisms, each playing a role in the scattering processes.

Recently published low branches of phonon dispersion curves[43,44,45,46], measured by neutron scattering, must be helpful for the phonon assignment of some of the Raman lines. According to these data, the strong 45 cm^{-1} line has an energy close to the energy of the zone center (ZC) TO_1 or the zone boundary (ZB) TA phonon. Lowering the temperature, TO_1 zone center phonon ex-

hibits softening, at T$\sim$T$_d$ K, due to the drastic increase of damping, it disappears. The overdamping continues down to T$_{do} \sim 210$ K[43]. It also causes significant, almost sixfold, broadening of the TA phonon branch[47]. It seems reasonable to expect that the Raman line at 45 cm^{-1} is also affected by the described phenomenon. However, none of the known Raman reports show any significant effects that could be attributed to this overdamping.

The formation of the lower-symmetry clusters in the host crystal is accompanied by relaxational and reorientational dynamics. This dynamics should be reflected in the light scattering spectrum either directly or through interaction with the phonon modes. Theoretical considerations[48] show that internal relaxational motion leads to the appearance of the central peak (CP) in the Raman spectrum. Interactions of this motion with phonons can cause softening of them[48]. These predictions have been tested on several types of crystals with internal degrees of freedom, like alkali-halide-cyanide (K(CN)$_x$-KBr$_{1-x}$, K(CN)$_x$-KCl$_{1-x}$)[49,50,51,52] compounds. Recently, we have analyzed[53] the reorientational motion in ferroelectric KTa$_{1-x}$Nb$_x$O$_3$ crystals. In this paper we discuss the role of the relaxational and reorientational dynamics in the scattering processes from PMN crystal.

In the paper presented we offer a complex analysis of temperature dependencies of polarized (VV) and depolarized (VH) Raman spectra from a single crystalline PMN sample. This analysis is based on multiple peak decomposition. An attempt to apply similar kind of analysis has earlier been made by Siny et al.[54]. But, it was restricted to the low frequency VV spectra in a limited temperature range (with maximum temperature $\sim$620 K), concentrating on the central peak (CP) only. To obtain the complete picture, we consider the temperature evolution of the whole Raman scattering spectrum (up to 1000 cm^{-1}) in the 100-1000 K temperature range. We interpret our results in connection with recently published neutron scattering data and with the concept of interaction of phonons with internal relaxational motion. As a result of this work, we present our view on the picture of structural transformations in PMN crystal and on the origin of its Raman spectrum.

II. EXPERIMENTAL SETUP AND RESULTS

We have investigated the Raman scattering from $\langle 100 \rangle$ cut PMN single crystal. The crystal was grown by the high temperature solution technique using 30 wt% PbO as flux. The growth conditions were optimized based on the pseudo-binary phase diagram established for PMN and PbO[55]. The as-grown crystal exhibits a pseudo-cubic morphology with $\langle 100 \rangle$ cub growth steps. A $\langle 100 \rangle$ / $\langle 110 \rangle$ cub-oriented crystal of a volume of 53 mm^3 was cut from a large as-grown crystal and polished with fine diamond paste (down to 0.25 mm). It showed very high optical quality and satisfied the requirements for light scattering

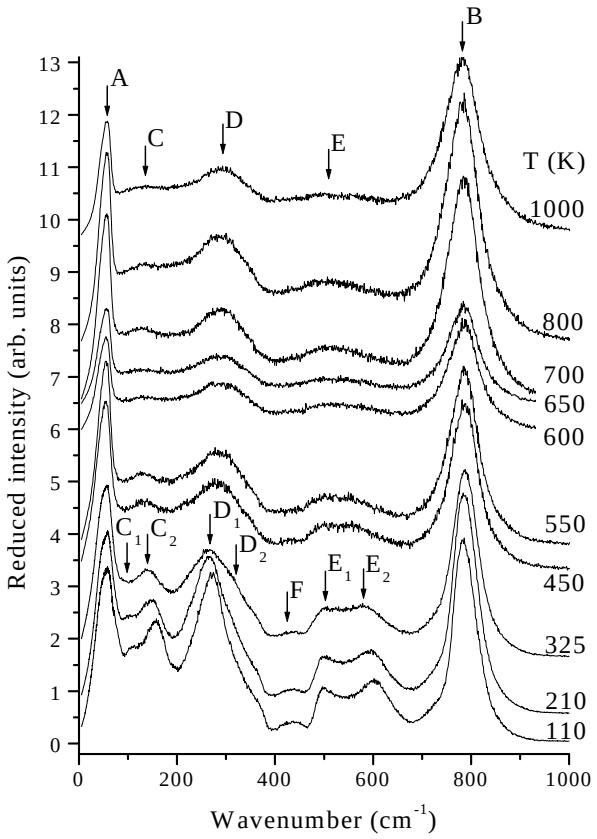

FIG. 1: Examples of Raman scattering spectra measured at various temperatures without polarization analysis and corrected by the population factor.

studies. The scattering was excited by propagating in $\langle 100 \rangle$ direction 514.5 nm light from a 200 mW Ar$^+$-ion laser, focused to a 0.1 mm spot. The scattered light was collected at an angle of 90° with respect to the incident beam (i.e., in $\langle 010 \rangle$ direction) by a double-grating ISA Jobin Yvon spectrometer equipped with a Hamamatsu photomultiplier R-649. For most of the measurements, the slits were opened to 1.7 cm^{-1}. However, in order to acquire more precise data in the central peak region, at the temperatures close to the maximum of the dielectric constant ($100 < T < 350$ K), the slits were narrowed to 0.5 cm^{-1}. Each polarization of the scattered light, $\langle x|zz|y \rangle$ (VV) and $\langle x|zx|y \rangle$ (VH), was measured separately. In order to exclude differences in sensitivity of the monochromator to different polarizations of the light, a circular polarizer was used in front of the entrance slit. For control purposes, we also took measurements without polarization analysis. Finally, to protect the photomultiplier from the strong Raleigh scattering, the spectral region from -4 to +4 cm^{-1} was excluded from the scans. The data were collected in the temperature range from

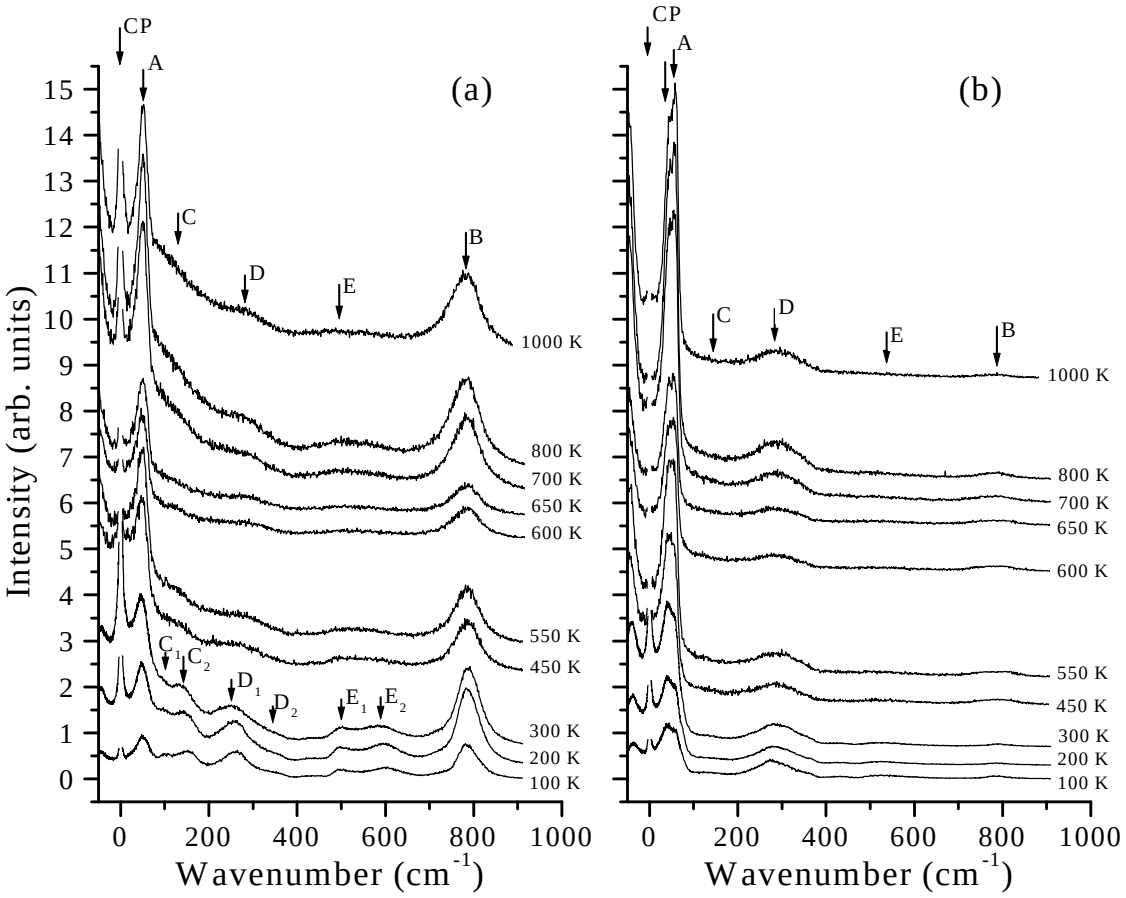

FIG. 2: Examples of Raman scatteting spectra measured in VV (a) and VH (b) geometries upon cooling from 1000 to 100 K.

1000 to 100 K. The cooling rate was 0.5-1 K/min. Every 50-20 K the temperature was stabilized and the spectrum recorded. We agree with Ref.[24] that the reproducibility of the spectra in the temperature range approximately between 200 and 350 K was not very good. In this range, the spectra exhibited a strong dependence on the cooling rate and other experimental conditions.

Fig.1 presents examples of light scattering spectra measured at different temperatures without polarization analysis. To facilitate comparison, we corrected the spectra by the Bose population factor:

$$F(f,T) = \begin{cases} n(f)+1, \text{ for Stokes part} \\ n(f), \text{ for anti-Stokes part} \end{cases}, \qquad (1)$$

where

$$n(f) = (exp(hf/kT) - 1)^{-1}.$$

Figure 2 demonstrates scattering spectra measured in VV (a) and VH (b) geometries at different temperatures. These spectra we present in uncorrected, "as-measured", form.

As can be seen from Figs. 1 and 2, our spectra are consistent with those from Refs.[14] and[24]. In the high temperature region, a typical spectrum consists of two strong lines centered approximately at 45 cm^{-1} and 780 cm^{-1} (labelled A and B) and of three broad bands (C, D, E). Line A exhibits fine structure, which is explicitly seen on the spectra measured with polarization analysis (see Figs. 2 and 3). Lowering temperature leads to the splitting of the broad bands C, D and E into a number of narrower lines (labelled by indices) and to appearance of new line F.

As seen from Fig. 1, starting from 1000 K, the reduced intensity of the scattering, first grows until the temperature of $\sim$ 700 K then sharply decreases to a minimum located close to the Burns temperature $T_d \approx 620$ K, after which it increases again. At $\sim$ 550 K its strength gets restored. Below this temperature, the intensities of the major lines (especially A and B) are determined primarely by the Bose factor. I.e. being corrected by it, they do not show significant temperature changes, demonstrat-

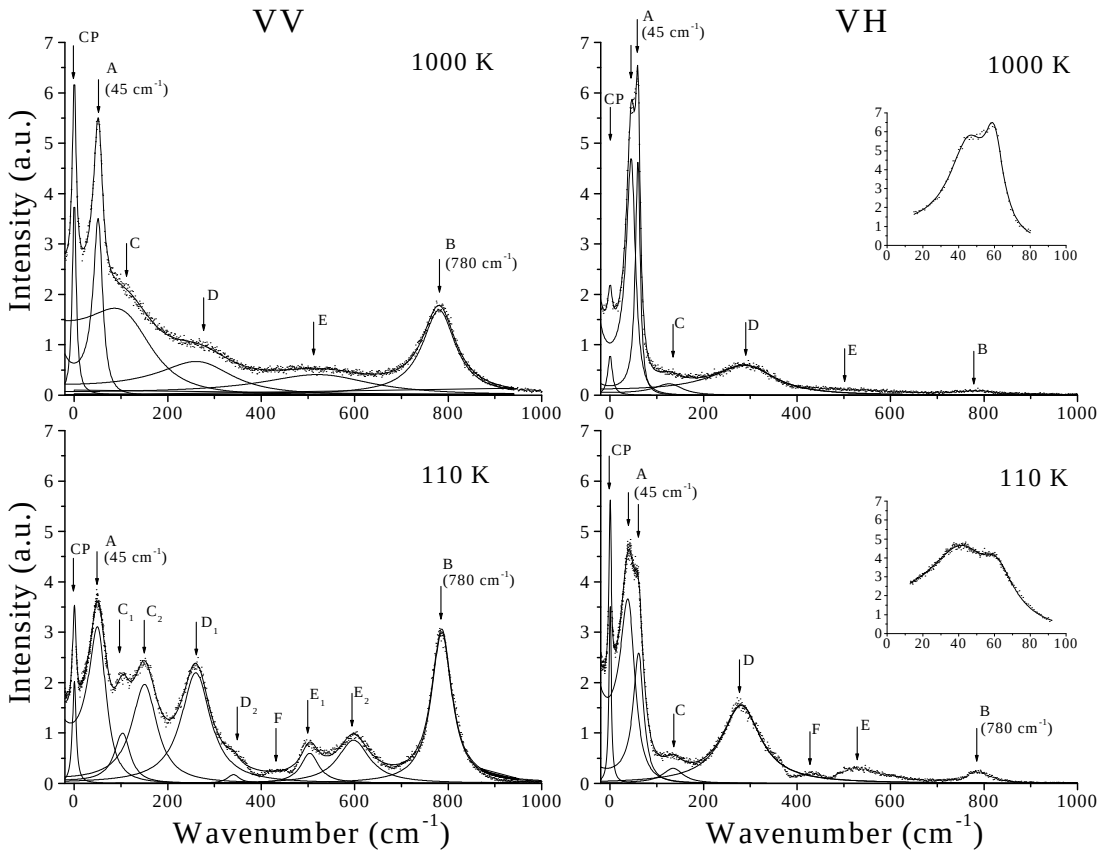

FIG. 3: Examples of multiple peak decomposition of Raman spectra measured at 1000 and 110 K both, in VV and VH geometry. For convenience, major peaks are labeled with letters. Inserts show examples of fits for the line A using the model of the two coupled harmonic oscillators, as described in Discussion.

ing characteristic first-order behavior. The shape similarity of the low- and high- temperature spectra shows that even at 1000 K the scattering has first-order character. In the perfecly cubic crystal, first-order scattering is prohibited. Therefore, one should assume the presence of distortions in the form of lower symmetry clusters, like Fm3m or R3m. At high temperature, these clusters might be present in the dynamic form, having short lifetime. Lowering the temperature, their lifetime increases and they become progressively more static. The observed around T_d decrease of Raman intensity is also clearly seen in Fig. 2. However, there are no reports on this effect in the literature; it might have been overlooked. This intensity drop indicates worsening of the optical quality of the crystal. In our opinion, it is consistent with the formation of Fm3m clusters in their evolution from dynamic to static form. The splitting of peaks is associated with the development of R3m clusters. The first signs of the splitting appear at T_d. Strarting from $T_f \sim 350$ K (which is also close to where the dispersion of the dielectric constant appears), this effect becomes even more definite and the intensities of the components begin to grow. Below $T_{do} \sim 210$ K, which is the temperature of electric field-induced ferroelectric phase transition[23] , the shape of the spectra is relatively stable.

A comprehensive analysis of our data and their comparison with results of other experiments allows to understand the meaning of the mentioned above temperatures $T_d \approx 620$ K, $T_f \approx 350$ K and $T_{do} \approx 210$ K in the temperature evolution of the Raman spectra and the lattice structure.

III. MULTIPLE-PEAK DECOMPOSITION OF SPECTRA PROCEDURE.

To be able to analyze the data, we decomposed the measured spectra using multiple peak fitting procedure. It was found that satisfactory fit could be achieved with the assumption that the central peak has a Lorentzian shape and that each of the other peaks is described by the spectral response function, i.e. damped harmonic oscillator, modified by the population factor (1):

$$\Phi_i \sim \frac{\Gamma_i f_{0i}^2 f}{(f^2 - f_{0i}^2)^2 + \Gamma_i^2 f_{0i}^2} F(f,T) \ , \qquad (2)$$

where Γ_i and f_{0i} are the damping constant and the mode frequency.

As all of the peaks are much better resolved at low temperatures, we started our fitting procedure at the low-temperature end of the data set (at 110 K) and, then, observed the evolution of the peaks with increasing temperature (i.e., in order, opposite to the order of measuring). At the same time, we tried to minimize the number of peaks necessary to achieve a reasonably good fit. The control data set (measured without polarization analysis) has been used to calibrate the positions and widths of the weak and poorely resolved peaks from the VV and VH data sets. Since a large number of parameters is involved, results of a particular fit may depend on their initial values. To stabilize the results, the best-fit values of parameters obtained at the previous temperature were used as initial values for the next one. In this manner, several sets of fits were obtained and analyzed. It is remarkable, that in all of them the major parameters showed the same trends of behavior, confirming the importance of the mentioned above temperatures: $T_d \approx 620 \pm 50$ K, $T_f \approx 350 \pm 25$ K and $T_{do} \approx 210 \pm 25$ K. These trends are summarized in Table II. One of the sets have been selected to report the most interesting results in detail. Examples of the fits at the temperatures of 1000 and 110 K in VV and VH geometries are shown in Fig. 3. For clarity, we describe the observed phenomena from high to low temperatures, following the same order as in measurements (unless the opposite stated).

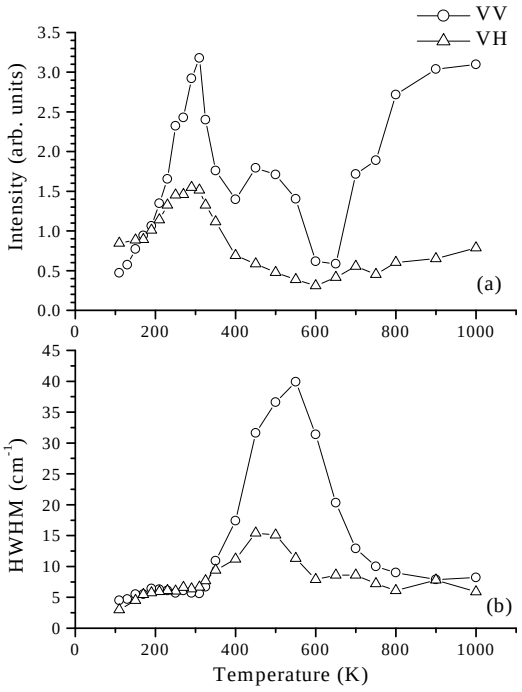

FIG. 4: Temperature dependencies of the intensity (a) and half-width (b) of the Lorentzian approximation for the central peak in VV (circles) and VH (triangles) geometries of experiment.

IV. MOST INTERESTING RESULTS OF DECOMPOSITION AND THEIR ANALYSIS.

A. Central peak.

The temperature dependences of the fitting parameters for the central peak (CP) are presented in Fig. 4. Circles correspond to the VV and triangles to the VH component of the peak. The existence of the CP is a direct consequence of the lattice relaxations, which are very sensitive to the restrictions imposed by the low-symmetry clusters. If relaxations are fast[48], the CP is low-intense and broad, whereas their slowing causes growth and narrowing of the peak.

We would like to point out a striking similarity of the temperature behavior of the CP in $PbMg_{1/3}Nb_{2/3}O_3$ (Fig. 4) and in $KTa_{0.85}Nb_{0.15}O_3$ (Fig.3 in Ref.[53]) crystals. We have shown[53] that the temperature behavior of the CP in KTN can be explained by the model involving the relaxational motion of off-centered Nb ions and its progressive restriction with temperature decrease. In the cubic phase, Nb ions are allowed to reorient amongst eight equivalent <111> directions. The appearance of the PNR's followed by a sequence of phase transitions down to a rhombohedral R3m phase, limits the ion motion to four, two and, finally, locks it in only one site. This model is in agreement with the diffuse neutron scattering studies of similar system[56]. The similarity of the CP behavior in these two very different materials, suggests that the temperature evolution of the polar clusters in $PbMg_{1/3}Nb_{2/3}O_3$ passes through the similar stages as in $KTa_{0.85}Nb_{0.15}O_3$ (KTN), however, it is not accompanied by appearance of the long-range order.

Starting from the high-temperature end (Fig. 4), the first important feature is the strong and narrow scattering in the VV geometry accompanied by a relatively weak scattering in the VH geometry. This indicates the presence of a symmetric slow relaxational motion, involving 180° reorientations of ions. Lowering the temperature, starting from $\sim$ 900 K, a cessation of this motion causes an intensity decrease of the CP. Slow at first, this decrease becomes sharper and reaches minimum near $T_d \approx 620$ K. The prohibition of 180o reorientations introduces anisotropy into the lattice causing the distinguishability between Mg and Nb occupied cites and to formation in the 1:1 ordered areas of the superstructure with, on average, Fm3m symmetry. It also imposes first restrictions on the reorientational motion of the dynamical R3m polar nanoregions. Now, they can reorient only amongst four neighboring <111> directions, forming, on average, tetragonal-like distortions. These processes are accompanied by the appearance of large (of the order of

TABLE II: Major peaks and their response to the temperature restrictions on ion motion. Only changing properties are shown. $T_d \approx 620$ K is also characterized by the total loss of intensity of scattered light.

Peak	Polarization	*Region I*. Unrestricted dynamical clusters $T \gtrsim (T_d=620\ K)$	*Region II*. Restricted dynamical clusters $(T_d=620\ K) \gtrsim T \gtrsim (T_{pr}=350\ K)$	*Region III*. Formation of static R3m clusters $(T_{pr}=350\ K) \gtrsim T$
Central	VV	Intensity decreases broadens	Intensity increases narrows	Intensity has a maximum at 300 K
	VH	Intensity decreases	Intensity increases width has a maximum at 450 K	Intensity has a maximum at 300 K
Peak A	VV		Softens, broadens	Hardens and narrows
	VH-I	Broadens	Broadens	Broadens
	VH-II	Softens	Hardens, intensity has minimum at 400 K	Broadens and grows
Peak C	VV	Hardens and narrows	Fine structure appears	Splits in two
	VH	Softens	Hardens and narrows	Narrows
Peak D	VV		Splits in two	
	VH	Softens	Hardens	Softens and narrows
Peak F	VV		VV component appears	VH component appears
Peak E	VV		Fine structure appears	Splits in two, VH appears
Peak B	VV	Hardening	Hardening	VH appears

wavelength of light) dynamic fluctuations causing worsening of the optical quality of the sample.

With further decrease of the temperature, the optical quality of the crystal improves. From $\sim$ 550 K, the four-cite reorientational motion of the PNR's starts to slow down, which is marked by the narrowing of the VV component of the CP and increase of its VV and VH intensities. The simultaneous broadening of the VH component up to the maximum at $\sim$ 450 K, indicates rearrangements in the crystalline structure leading to the appearance of the new type of restrictions on the ion motion. Analogy with KTN suggests that below $\sim$ 450 K the motion of R3m clusters becomes limited to two neigboring <111> orientations, averaging in monoclinic-like distortions. Such a rearrangement causes some decrease in intensity of the VV component (with minimum at $\sim$ 400 K), while the VH intensity keeps growing. Below $\sim$ 400 K, the slowing down of the two-site relaxational motion causes narrowing the CP and increase of intensities of both components. From $T_f \approx 350$ K, these effects become especially dramatic. Further temperature decrease, starting from $\sim$ 300 K, leads to the complete prohibition of intersite reorientational motion of R3m clusters, i.e. to appearance of static R3m clusters. This is marked by a sharp decrease in intensity of both components of the CP. At the temperature $T_{do} \approx 210$ K, the process of conversion of PNR's from dynamic to static form (freezing) is primarily finished. Below this temperature, the central peak is narrow and its intensity is small in both scattering geometries.

We should mention that the result of our analysis of the VV component of the CP exhibits similar tendencies to those in Ref.[54], except at the low temperature end. The discrepancy occurs due to the difference in experimental technique. In the central peak region, we did the measurements with much higher resolution (0.5 cm^{-1}, as compared to 2 cm^{-1} from Ref.[54]). Consequently, we were able to provide a more correct separation of the slow relaxations from the elastic scattering, which was especially important at low temperatures.

B. Line A.

Figure 5 presents the temperature evolution of the fitting parameters of the peak A, showing its position (a), reduced intensity (b) and damping constant (c). This peak has a triplet structure, containing one component in VV (circles) and two components in VH (up and down triangles) geometries. The fitting parameters for this peak exhibit changes at mentioned above temperatures T_d, T_f and T_{do}, confirming their importance for the structural evolution of the crystal. However, the origin of this peak (see Table. I) requires qlarification. From a comparison with the frequencies of the phonon modes determined from neutron scattering, it is clear that this line cannot be due to the zone center soft TO_1 mode (black stars in Fig. 5). On the other hand, the lower frequency VH component, and possibly the VV component could be due to the disorder-induced zone boundary scattering on TA phonon (white stars in Fig. 5). However, the higher frequency VH component would still not be accounted for.

In an attempt to account for both VH components simultaneously, we have tried to make use of a coupled oscillator model. In the approximation of linear coupling

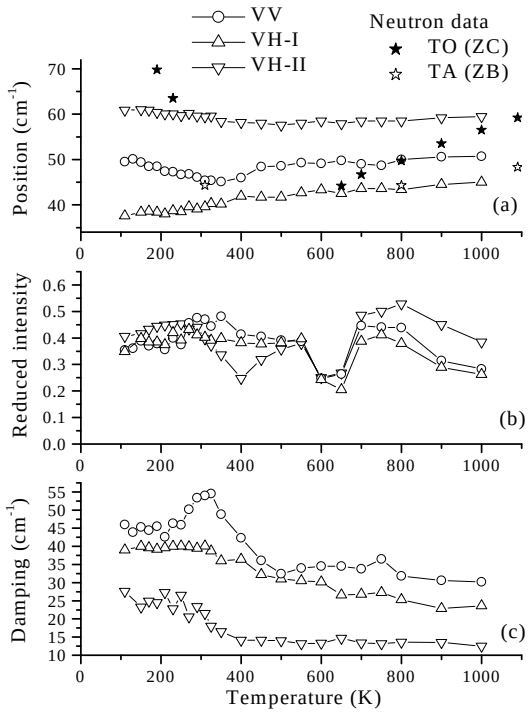

FIG. 5: Temperature dependences of the fitting parameters: position (a), reduced intensity (b) and damping constant (c) for the triplet line A (located at around 45 cm^{-1}). Phonon frequencies, measured by neutron spectroscopy[43,44,45,46], are shown for comparizon.

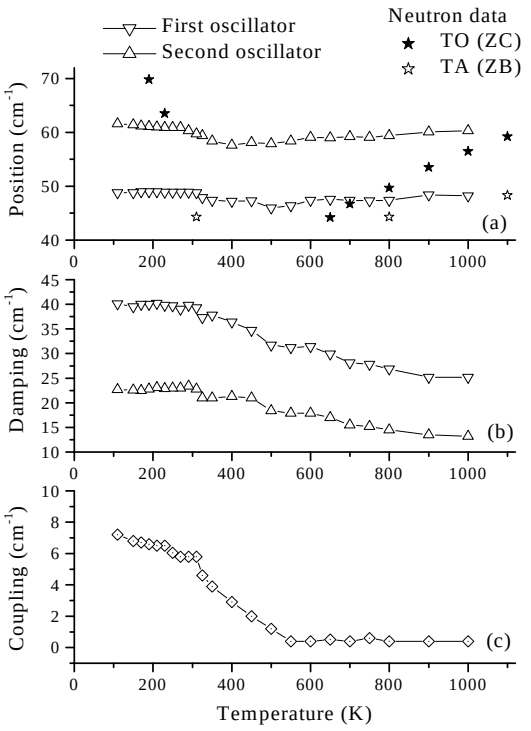

FIG. 6: Temperature dependences of the fitted parameterst of the line A VH component (located at 45 cm^{-1}) using the model of coupled harmonic oscillators. From top to bottom: resonant frequencies (a), damping constants (b) and coupling constant (c). Phonon frequencies, measured by neutron spectroscopy[43,44,45,46], are shown for comparizon.

between two harmonic oscillators[57] this approach gains:

$$I(\omega) = [n(\omega)+1]\left(\frac{CY - BZ}{B^2 + C^2}\right),$$

where

$B = (\omega_1^2 - \omega^2)(\omega_2^2 - \omega^2) + \omega^2(\gamma_{12}^2 - \gamma_1\gamma_2) - \omega_1\omega_2\Delta_{12}^2,$
$C = \omega[\gamma_1(\omega_2^2 - \omega^2) + \gamma_2(\omega_1^2 - \omega^2) - 2(\omega_1\omega_2)^{1/2}\Delta_{12}\gamma_{12}],$
$Y = S_1^2(\omega_2^2 - \omega^2) + S_2^2(\omega_1^2 - \omega^2) - 2S_1S_2(\omega_1\omega_2)^{1/2}\Delta_{12},$
$Z = \omega(S_1^2\gamma_2 + S_2^2\gamma_1 - 2S_1S_2\gamma_{12}).$

In these equations ω_1 and ω_2 are the resonant frequencies, γ_1 and γ_2 are the damping constants, S_1 and S_2 are the structure factors for two oscillators, Δ_{12} and γ_{12} are the real and imaginary parts of the coupling constant.

It was shown[58], that a unitary transformation can be found, which would set either real or imaginary part of the coupling to be equal to zero. We have chosen to use imaginary coupling and set $\Delta_{12} = 0$. We also set the structure factors S_1 and S_2 to be the same at all temperatures. The rest of the parameters were treated as being temperature dependent. In the result of fitting, we have found that the values of structure factors can be approximated as $S_1 = 22.3$ cm^{-1} and $S_2 = 20.6$ cm^{-1}. The other parameters as a function of temperature are shown in Fig.6: the best-fit frequencies (a), the damping constants (b) and the coupling coefficient (c).

The examples of the fits (inserts in Fig.3) demonstrate that this model gives a good approximation to the shape of the peak A. However, a comparizon of the best-fit frequencies (Fig. 6a) with the neutron scattering data[43,44,45,46] rules out the possibility to explain the higher-frequency VH component by the interaction between ZC TO_1 (black stars) and ZB TA (white stars) modes. The lower frequency oscillator can still be associated with disorder-induced scattering on ZB TA mode.

The possible explanation of the presence of two VH components in the peak A can be in the correspondence to TA modes with different polarizations in different crystalline planes of a distorted lattice. (A similar effect we have seen in monodomain $KTa_{1-x}Li_xO_3$, where one or the other TA polarization was observed, depending on the orientation of the electric field.) These differently polarized modes are influenced by the polar nanoregions, which explains the increase of damping (Fig. 6b) and coupling (Fig. 6c) coefficients with lowering temperature.

It is also necessary to point out an observation concerning the temperature dependences of the frequencies of the components of the triplet A in approximation of independent oscillators (Fig. 5a). These dependences seem to show anomalies at intersections with ZC TO_1 modes (black stars). For example, the VV component exhibits deeps at $\sim$ 700 and 350 K and VH-I component has a knee at $\sim$ 400 K.

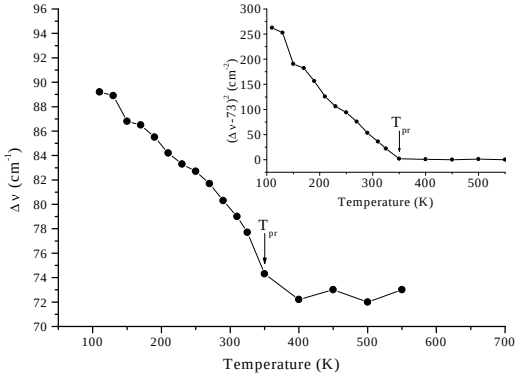

FIG. 7: Amplitude of splitting between the components of the line E. The insert demonstrates that this splitting follows the critical dependence.

C. The most important parameters of other lines.

Among the changes occuring to the Raman spectrum with cooling the sample, the splitting of the phonon lines desrves special attention, since such a splitting is a direct indicator of the modifications of the local structure. As we already mentioned, the splitting occurs to the lines C, D, and E, which is especially well seen in the VV geometry (Fig. 2a). At high temperatures, their widths are very big, so the lines almost merge in a single broad shoulder. Lowering the temperature, they become more discernible and the fine structure gradually develops. The first signs of it appear at $T_d \approx 620$ K. Below $T_{pr} \approx 350$ K, the fine structure becomes more obvious. These observations support the expressed above idea that the scattering originates from the distorted regions. Highly dynamic and disordered at high temperature, they become progressively more static with cooling down, and their motion becomes more correlated. This process is reflected by the temperature evolution of the lines C, D, and E.

Below the temperature of $T_{pr} \approx 350$ K, the splitting value of the line E exhibits especially interesting trend. As seen from Fig. 7, with temperature decrease below T_{pr} the distance between the E-line components increases. Moreover, this increase exhibits the characteristic order parameter behavior, following the $(T_{pr}-T)^{-1/2}$ dependence, which is demonstrated in the insert to Fig. 7. It also exhibits similar temperature tendency to that described in Ref.[59]. Detailed understanding of this phenomenon requires further work, and it is a subject of separate paper.

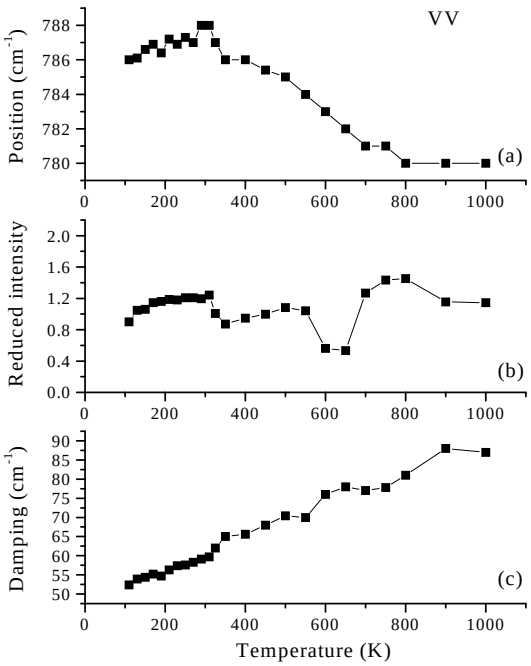

FIG. 8: Temperature dependencies of the fitting parameters: position (a), reduced intensity (b) and damping constant (c) of the line B (located at $\sim$780 cm^{-1}.)

Finally, we would like to stop on the line B located at the upper end of the spectrum. Fig. 8 demonstrates the fitting paramenters for this line: position (a), reduced intensity (b), and damping coefficient (c). This line is very strong in the VV geometry but it is rather weak in the VH one (i.e. characterized by A_{1g} symmetry). It seems to be the least influenced by the ordering processes in the crystal. However, the temperature evolution of its parameters reflects development of the low-temperature phase, confirming the expressed above ideas about formation of dynamic polar clusters at $T_d \approx 620$ K, their slowing down, and appearance of the static order at $T_{pr} \approx 350$ K. As it is seen from the Table I, the appearance of this line in the Raman spectrum has several contradictory explanations. However, according to the recent first-principle calculations[42], this mode most likely is a consequence of oscillations of oxygen ions.

V. CONCLUSION

This paper offers a comprehensive analysis of the Raman scattering spectra of $PbMg_{1/3}Nb_{2/3}O_3$ in the temperature range between 100 and 1000 K. From our analysis, the structural evolution of the lattice occurs in several stages. Even at 1000 K, the PMN crystal is characterized by the presence of dynamic distortions of the lattice from cubic symmetry, which are responsible for existence of first-order Raman scattering at such a high temperature. At the Burns temperature $T_d \approx 620$ K, the first restrictions on the reorientational motion of the off-centered ions appear. These restrictions lead to slowing of the motion and growth of correlations between neighboring regions with R3m symmetry. They also introduce distinguishability between sites occupied by Mg and Nb, which causes onset of Fm3m symmetry in the 1:1 ordered areas. Further cooling leads to progressive growth of restrictions on ionic motion and, starting from $T_{pr} \approx 350$ K, to the appearance of the static polar nanoregions. At $T_{do} \approx 210$ K, the formation of the low-temperature phase is primarily finished. The shape of the phonon lines is determined by multiphonon processes involving phonons with different polarizations propagating in different directions, which interact with dynamic and static disorder.

VI. ACKNOWLEDGEMENT

Authors are very grateful to D.La-Orauttapong and G.Yong for useful advice and helpful discussions. This work was partially supported by the ONR grant #N00014-99-1-0738.

* On leave from the Institute of Semiconductor Physics, Kyiv 03028, Ukraine

[1] V.A.Bokov, I.E.Myl'nikova, Sov. Phys. - Solid State, **3**, 613 (1961).

[2] D.Viehland, S.Jang, L.E.Cross, Phil. Mag. B, **64**, 335 (1991).

[3] D.Viehland, S.J.Jang, L.E.Cross, M.Wuttig, Phys. Rev. B, **46**, 8003 (1992).

[4] J.Chen, H.M.Chan, M.P.Harmer, J. Am. Ceram. Soc., **72**, 593 (1989).

[5] C.Boulesteix, V.Varnier, A.Llebaria, E.Husson, J. Sol. State Chem., **108**, 141 (1994).

[6] S.Miao, J.Zhu, X.Zhang, Z.-Y.Cheng, Phys. Rev. B, **65**, 052101 (2001).

[7] E.Husson, M.Chubb, A.Morell, Mat. Res. Bull., **23**, 357 (1988).

[8] A.D.Hilton, D.J.Barber, C.A.Randall, T.R.Shrout, J. Mat.Sci., **25**, 3461 (1990).

[9] M.A.Akbas, P.K.Davies, J. Am. Ceram. Soc., **83**, 119 (2000).

[10] P.K.Davies, M.A.Akbas, J. Phys. Chem. Solids, **61**, 159 (2000).

[11] R.Blinc, A.Gregorovic, B.Zalar, R.Pirc, V.V.Laguta, M.D.Glinchuk, Phys. Rev. B, **63**, 024104 (2001).

[12] I.W.Chen, J. Phys. Chem. Solids, **61**, 197 (2000).

[13] T.Egami, W.Dmowski, M.Akbas, P.K.Davies, First-Principles Calculations for Ferroelectrics, ed. by R.E.Cohen, Fifth Williamsburg Workshop, Williamsburg, VA February 1998, AIP Conf. Proc., **436**, p.1 (1998).

[14] E.Husson, L.Abello, A.Morell, Mat. Res. Bull., **25**, 539 (1990).

[15] G.Burns, F.H.Dacol, Solid St. Commun., **48**, 853 (1983) and Phys. Rev. B., **28**, 2527 (1983).

[16] N.Takesue, Y.Fujii, H.You, Phys. Rev. B, **64**, 184112 (2001).

[17] J.Toulouse, P.DiAntonio, B.E.Vugmeister, X.M.Wang, L.A.Knauss, Phys. Rev. Lett. **68**, 232 (1992).

[18] P.Bonneau, P.Garnier, G.Calvarin et al., J. Solid State Chem., **91,** 350 (1991).

[19] N.de Mathan, E.Husson, G.Calvarin, J.R.Gavarri, A.W.Hewat, A.Morell, J. Phys.: Condens. Matter, **3**, 8159 (1991).

[20] A.Verbaere, Y.Piffard, Z.-G. Ye, E.Husson, Mat. Res. Bull., **27**, 1227 (1992).

[21] Y.Uesu, H.Tazawa, K.Fujishiro, Y.Yamada, J. Korean Physical Society, **29**, S703 (1996).

[22] S.Vakhrushev, S.Zhukov, G.Fetisov, V. Chernyshov, J. Phys.: Condens. Matter, **6**, 4021 (1994).

[23] Z.-G.Ye, H.Schmid, Ferroelectrics, **145**, 83 (1993).

[24] H.Ohwa, M.Iwata, N.Yasuda, Y.Ishibashi, Ferroelectrics, **229**, 147 (1999); **218**, 53 (1998).

[25] G.Burns, B.A.Scott, Solid St. Commun., **13**, 423 (1973).

[26] N.N.Krainik, L.A.Markova, A.A.Karamjan, Ferroelectrics **143**, 179 (1993).

[27] M.El Marssi, R.Farhi, X.Dai, A.Morell, D.Viehland, J. Appl. Phys. **80**(2), 1079 (1996).

[28] M.El Marssi, R.Farhi, D.Viehland, J. Appl. Phys. **81**(1), 355 (1997).

[29] M.El Marssi, R.Farhi, M.D.Glinchuk, L.Sedun, D.Viehland, J. Appl. Phys. **83**(10), 5371 (1998).

[30] M.El Marssi, R.Farhi, Yu.I.Yuzyuk, J. Phys.: Cond. Matter. **10**, 9161 (1998).

[31] I.Dujovne, T.-Y.Koo, A.Pinczuk, S.-W.Cheong, B.S.Dennis, Phys. Rev. B, **66**, 064110 (2002).

[32] F.Jiang, S.Kojima, Jpn. J. Appl. Phys. **38**, 5128 (1999).

[33] S.G.Lushnikov, S.N.Gvasalia, I.G.Siny, Physica B, **263-264**, 286 (1999).

[34] S.G.Lushnikov, S.N.Gvasalia, I.G.Siny, E.A.Goremychkin, I.L.Sashin, Ferroelectrics, **236**, 147 (1999).

[35] I.G.Siny, R.S.Katiar, S.G.Lushnikov, Mat. Res. Soc. Symp. Proceedings, Vol. 457, 39.

[36] I.G.Siny, R.S.Katiar, A.S.Bhalla, J. Raman Spectroscopy, **29**, 385 (1998).

[37] I.G.Siny, S.G.Lushnikov, R.S.Katiar, Ferroelectrics, **231**, 115 (1999).

[38] I.G.Siny, R.S.Katiar, Ferroelectrics, **223**, 35 (1999).

[39] I.G.Siny, S.G.Lushnikov, R.S.Katiar, V.H.Schmidt, Ferroelectrics, **226**, 191 (1999).

[40] H.Idink, W.White, J. Appl. Phys. **76**, 1789 (1994).

[41] V.Dimza, P.Paulins, M.S.Zhang, Q.Chen, Z.Lin, Ferroelectrics **131**, 239 (1992).
[42] S.Prosandeev. Private communication.
[43] P.M.Gehring, S.Wakimoto, Z.-G.Ye, G.Shirane, Phys. Rev. Lett. **87**, 277601 (2001).
[44] S.Wakimoto, C.Stock, Z.G.Ye, W.Chen, P.M.Gehring, G.Shirane, arXiv:cond-mat/0112366.
[45] P.M.Gehring, S.B.Vakhrushev, G.Shirane, AIP Conf. Proc. Fundamental Physics of Ferroelectrics 2000. Aspen. Winter Workshop, 314 (2000).
[46] A.Naberezhnov, S.Vakhrushev, B.Dorner, D.Strauch, H.Moudden, Eur. Phys. J. B **11**, 13 (1999).
[47] T.-Y.Koo, P.M.Gehring, G.Shirane, V.Kiryukhin, G.Lee and S.-W.Cheong, arXiv:cond-mat/0110531 v1, 25 Oct 2001.
[48] K.H.Michel, J.Naudts, B.De Raedt. Phys. Rev. B, **18**, 648 (1978).
[49] J.M.Rowe, J.J.Rush, E.Prince, J.Chem.Phys. **66**, 5147 (1977).
[50] J.M.Rowe, J.J.Rush, S.Susman, Phys.Rev. B **28**, 3506 (1983).
[51] F.Luty, in *Defects in Insulating Crystals*, edited by V.M.Tuchkevich and K.K.Shvarts (Zinatne Publishing House, Riga, 1981) p.70.
[52] F.Luty, Phys.Rev.B **10**, 3677 (1974).
[53] O.Svitelskiy, J.Toulouse, accepted to JPCS.
[54] I.G.Siny, S.G.Lushnikov, R.S.Katiyar, E.A.Rogacheva, Phys.Rev.B., **56**, 7962 (1997).
[55] Z.-G. Ye, P. Tissot and H. Schmid, Mater. Res. Bull., **25**, 739 (1990).
[56] G.Yong, J.Toulouse, R.Erwin, S.M.Shapiro, B.Hennion, Phys.Rev. B 62 (2000) 14736.
[57] R.Currat, H.Buhay, C.H.Perry, A.M.Quittet, Phys. Rev. B, **40**, 10741 (1989).
[58] A.S.Barker, J.J.Hopfield, Phys. Rev., **135**, A1732 (1964).
[59] I.P. Raevski, S.A. Prosandeev, U. Waghmare, V.V. Eremkin, V.G. Smotrakov, V.A. Shuvaeva. ArXiv cond-mat/0208116.